SCIENCE CHINA
Information Sciences

• RESEARCH PAPER •

October 2025, Vol. 68, Iss. 10, 202402:1–202402:7
https://doi.org/10.1007/s11432-024-4460-y

High-performance SiN/AlGaN/GaN MIS-HEMTs on Si substrate with LPCVD-SiN passivation and n^+-InGaN ohmic contacts

Mengdi LI[1], Jiejie ZHU[1*], Sheng ZHANG[2], Bowen ZHANG[1], Yuxi ZHOU[1], Dayan YUAN[1], Lingjie QIN[1], Mingchen ZHANG[1], Qingyuan CHANG[1], Chupeng YI[1], Ke WEI[2], Xinyu LIU[2], Xiaohua MA[1] & Yue HAO[1]

[1]*State Key Discipline Laboratory of Wide Band-gap Semiconductor Technology, Xidian University, Xi'an 710071, China*
[2]*Institute of Microelectronics, Chinese Academy of Sciences, Beijing 100029, China*

Received 10 December 2024/Revised 5 March 2025/Accepted 23 May 2025/Published online 10 September 2025

Abstract In this work, we present high-performance SiN/AlGaN/GaN metal-insulator-semiconductor high electron mobility transistors (MIS-HEMTs) on Si substrate for low-voltage application. Attributed to n^+-InGaN regrown ohmic contacts, the devices show low on-resistance of 0.6 Ω·mm and knee voltage of 1.2 V. Low pressure chemical vapor deposition SiN was used as a passivation to withstand the high temperature when SiN gate dielectric was deposited by plasma enhanced atomic layer deposition. The devices with the source-drain spacing of 0.9 μm demonstrate low leakage current with the high on/off current ratio of 5×10^7, breakdown voltage of 52 V, and low current collapse at 30 V drain quiescent condition of 3.5%. Due to the use of 7-nm thin-barrier AlGaN, the devices with a 250-nm gate length have gradely frequency characteristics with a peak transconductance of 597 mS/mm and a cut-off frequency/maximum oscillation frequency (f_T/f_{max}) of 43/120 GHz. S-band continuous wave large signal measurements yield a high PAE over 70% at low voltages of 6 and 9 V. The devices show a maximum output power of 1.73 W/mm and power gain of 19.1 dB at $V_{ds} = 9$ V. These excellent performances reveal the great potential of the SiN/AlGaN/GaN MIS-HEMTs in low-voltage RF applications.

Keywords GaN metal-insulator-semiconductor high electron mobility transistors (MIS-HEMTs), low pressure chemical vapor deposition SiN, regrown ohmic, Si substrate, low-voltage RF applications

Citation Li M D, Zhu J J, Zhang S, et al. High-performance SiN/AlGaN/GaN MIS-HEMTs on Si substrate with LPCVD-SiN passivation and n^+-InGaN ohmic contacts. Sci China Inf Sci, 2025, 68(10): 202402, https://doi.org/10.1007/s11432-024-4460-y

1 Introduction

GaN-based high electron mobility transistors (HEMTs) have the advantages of high breakdown voltage, high output power, fast switching speed, high temperature resistance, and radiation resistance, which have attracted wide attention in 5G communication, radar, satellite communication, power electronics and so on [1–3]. The existing GaN RF power devices are mainly used in high operating voltage and high output power scenarios, so as to give full play to the advantages of GaN technology to improve the coverage ability of RF signals [4–6]. GaAs RF technology with advantages of cost and maturity is still more used in low-voltage application scenarios such as mobile communication terminals, microbase stations, and wearable devices [7, 8]. However, GaN HEMTs also have great potential in low-voltage applications, which is attributed to the advantages of high output power density and high power additional efficiency [9–11]. What is more, Intel reports that GaN-based HEMTs have lower on-resistance than Si-based devices at the same breakdown voltage and are superior to GaAs RF devices at low operating voltages in terms of power additional efficiency and output power density [12].

The key issues in achieving high performance GaN HEMTs at low voltage have two factors. (i) Increasing power additional efficiency by reducing the leakage current of the devices and joule heat dissipation. (ii) Increasing the power output density of the devices by reducing the parasitic resistance and enhancing the output current density. The off-state leakage current includes buffer leakage current

* Corresponding author (email: jjzhu@mail.xidian.edu.cn)

and gate leakage current, in which buffer leakage current and gate leakage current can be suppressed by the technology of back barrier and the introduction of gate medium or plasma treatment in the gate region, respectively [13–15]. The parasitic resistance consists of contact resistance and access resistance. The lower contact resistance could be achieved through the technical route of n^+-GaN/InGaN regrowth, deposition of Si before the ohmic metal evaporates, and ion implantation in the ohmic regions [16–18]. Furthermore, the adoption of strongly polarized heterojunctions, such as AlN/GaN and InAlN/GaN, scaling down the source-drain distance can effectively reduce access resistance [19, 20].

The development of GaN HEMTs on Si substrate faces challenges such as thermal and lattice mismatches, resulting in defects (cracks and dislocations) and self-heating [21–24]. However, advancements in buffer layer engineering, field plate technology, and the use of Si wafers for cost-effective production have significantly improved both performance and commercial feasibility. Soni et al. [25] designed multiple drain-connected field plates, which doubled the breakdown voltage to over 300 V. Gustafsson et al. [26] implemented stepped Carbon doping in the buffer layer, achieving low leakage currents in the off-state while avoiding current collapse, resulting in an f_{T} of 46 GHz and an $f_{\max}$ of 146 GHz. On the other hand, GaN HEMTs on Si substrate have great advantages of low cost and large wafer size, which can promote the popularization and application of 5G communication and other emerging technologies [27–29]. In addition, the heterogeneous integration of GaN RF devices and silicon transistors can also be realized on Si process platform, so as to greatly improve the electrical circuit performance and integration density and promote the development of intelligent front-end chip technology [30, 31]. The advantage of the low cost of GaN HEMTs on Si substrate is that they can meet the core needs of RF devices for low-voltage applications. However, GaN HEMTs on Si substrate using AlGaN barrier, which is the most mature barrier material and the closest to industrialization, have rarely been reported for low-voltage RF applications.

In this paper, n^+-InGaN regrown ohmic method and low-pressure chemical vapor deposition (LPCVD) SiN passivation were adopted to realize high-performance SiN/AlGaN/GaN MIS-HEMTs on Si substrate. LPCVD-SiN passivation was used for the first time in GaN HEMTs for low-voltage RF applications. Although similar passivation methods have been reported, only the use of LPCVD-SiN in medium and high voltages was studied, and the great potential of LPCVD-SiN in low-voltage RF applications was ignored [32, 33]. Benefiting from scaling down the source-drain distance (L_{sd}) to 0.9 μm to further reduce the access resistance, a low on-resistance (R_{on}) of 0.6 Ω·mm with a high saturation current density of 1.2 A/mm and a low knee voltage (V_{knee}) of 1.2 V were obtained for the SiN/AlGaN/GaN MIS-HEMTs. Plasma-enhanced atomic layer deposition (PEALD) SiN gate dielectric was adopted to greatly decrease gate leakage current by about three orders compared to the AlGaN/GaN Schottky-gate HEMTs. Pulsed *I*-*V* measurement shows that a low current collapse at 30 V drain quiescent condition of 3.5% was achieved for the SiN/AlGaN/GaN MIS-HEMTs. High PAE of 71% (70.6%) and a high maximum output power density (P_{out}) of 0.91 W/mm (1.73 W/mm) at low drain voltages of 6 V (9 V) in a continuous-wave (CW) mode at 3.6 GHz have been achieved with the SiN/AlGaN/GaN MIS-HEMTs.

2 Device structures and fabrication

The schematic cross-sectional of the SiN/AlGaN/GaN MIS-HEMTs is shown in Figure 1(a). The AlGaN/GaN HEMT wafer was grown by metal-organic chemical vapor deposition (MOCVD) on a 6-inch high resistance (HR) Silicon. A 1-μm GaN buffer was grown on a Si substrate, followed by a 150-nm undoped GaN channel layer. The AlGaN barrier consists of a 1-nm GaN cap layer, a 7-nm AlGaN barrier layer, and a 1-nm AlN interface enhancement layer. A 110-nm SiN was grown by LPCVD as a passivation layer and a mask of regrown ohmic. On-wafer Hall measurement yields a sheet resistance of 276 Ω/square, a sheet carrier density of 1.08×10^{13} cm^{-2}, and an electron mobility of 2064 cm^2/V·s.

As shown in Figure 1(b), the device fabrication process began with the deposition of the SiO_2 by plasma enhanced chemical vapor deposition (PECVD), which together with LPCVD-SiN acts as a mask of regrown ohmic. Then, the PECVD-SiO_2 and LPCVD-SiN on the ohmic region were removed by the F-based inductively coupled plasma etching. The n^+-InGaN was regrown on the whole wafer by MOCVD to reduce the ohmic contact resistance of the devices. After that, PECVD grown SiO_2 mask was removed by diluted HF solution, while the LPCVD-SiN was retained due to the slower corrosion rate. Therefore, the use of LPCVD-SiN passivation can make GaN HEMTs with regrown ohmic not be damaged by HF solution on the surface of AlGaN/GaN heterostructure when removing the mask. Then,

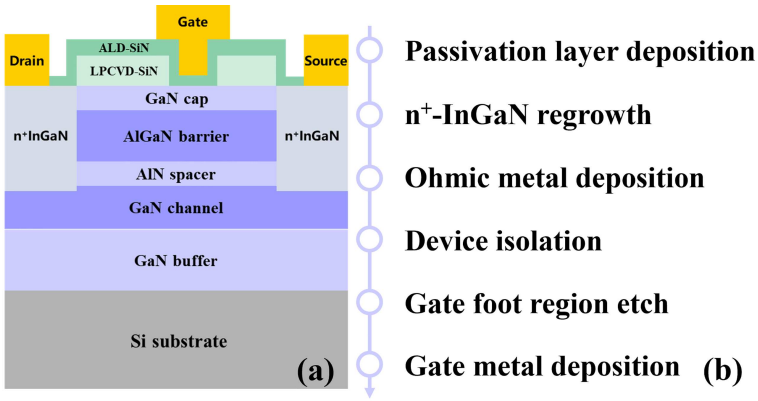

Figure 1 (Color online) (a) Schematic cross-sectional and (b) fabrication process flow of the SiN/AlGaN/GaN MIS-HEMTs.

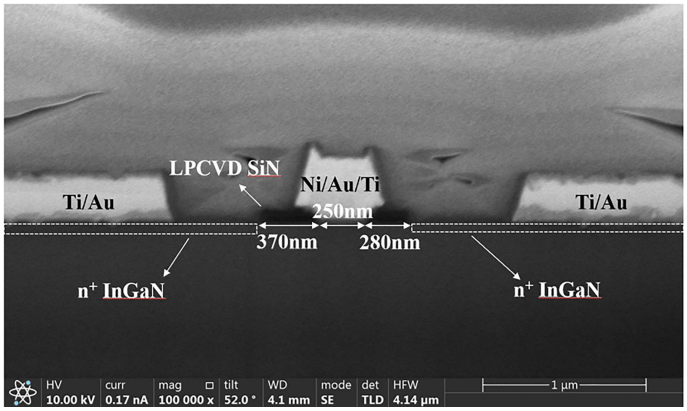

Figure 2 (Color online) Cross-sectional SEM picture of the SiN/AlGaN/GaN MIS-HEMTs.

Ti/Au metal stacks were deposited as ohmic contact formation. The LPCVD-SiN on the mesa isolation region was removed by the F-based inductively coupled plasma reactive ion etching, followed by nitrogen implantation to isolate the active region of the devices. Transmission line models were used to evaluate the resistance component for the regrown structure. The low ohmic contact resistance of 0.17 Ω·mm was measured. Then, the gate recess window was defined by etching LPCVD-SiN with F-based inductively coupled plasma etching, followed by the deposition of a 5-nm PEALD-SiN. Finally, the gate fabrication was finished by the deposition of Ni/Au/Ti metal stacks. Figure 2 shows the cross-sectional SEM picture of the SiN/AlGaN/GaN MIS-HEMTs. The fabricated SiN/AlGaN/GaN MIS-HEMTs feature a source-drain distance ($L_{\rm sd}$) of 0.9 µm, a gate length ($L_{\rm g}$) of 250 nm, a gate-source spacing ($L_{\rm gs}$) of 280 nm, a gate-drain spacing ($L_{\rm gd}$) of 370 nm, and a total gate width of 2 × 25 µm. The devices with the same fabrication process and structure dimension as SiN/AlGaN/GaN MIS-HEMTs without the PEALD-SiN gate dielectric, i.e., AlGaN/GaN Schottky-gate HEMTs, were fabricated for comparison.

3 Results and discussion

Figure 3(a) shows the transfer curves of the SiN/AlGaN/GaN MIS-HEMTs and AlGaN/GaN Schottky-gate HEMTs measured in double mode at $V_{\rm ds}$ = 6 V. For the SiN/AlGaN/GaN MIS-HEMTs, $V_{\rm th}$ was extracted to be −1.0 V by linear extraction and small $V_{\rm th}$ hysteresis less than 0.06 V was achieved. Here, the negative shift of the $V_{\rm th}$ of the SiN/AlGaN/GaN MIS-HEMTs compared to the AlGaN/GaN Schottky-gate HEMTs is mainly attributed to the decreased control ability of the gate over the two-dimensional electron gas (2DEG) channel due to the introduction of the gate dielectric, which can also be verified by the reduction of the peak transconductance from 823 to 597 mS/mm. The excessively large leakage current of 5 × 10^{-2} mA/mm results in a relatively low on/off current ratio of 2 × 10^4 for the AlGaN/GaN Schottky-gate HEMTs. On the contrary, the SiN/AlGaN/GaN MIS-HEMTs exhibit a lower off-state current of 2 × 10^{-5} mA/mm and a high on/off current ratio over 5 × 10^7, suggesting

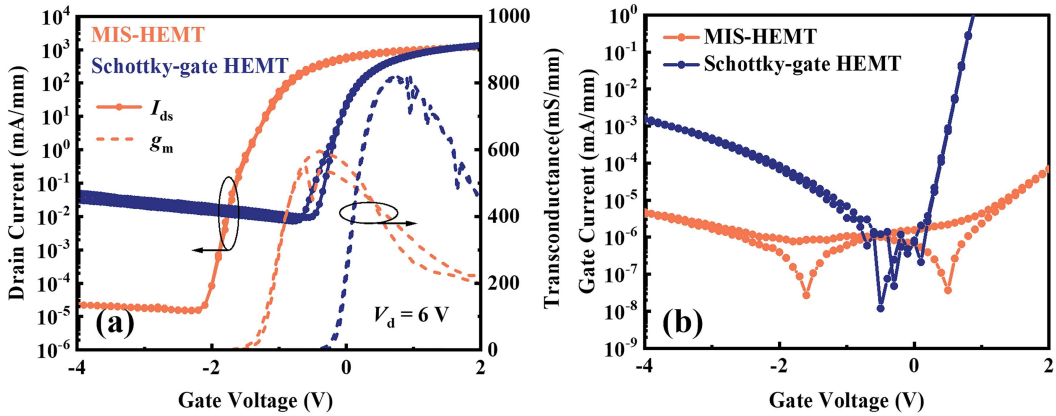

Figure 3 (Color online) (a) Transfer and (b) gate diode characteristics of SiN/AlGaN/GaN MIS-HEMTs and AlGaN/GaN Schottky-gate HEMTs on 6-inch HR-Si substrates.

a superior vertical leakage current blocking capability of the PEALD-SiN gate dielectric. Figure 3(b) compares the gate leakage currents under the reverse and forward gate biases for the SiN/AlGaN/GaN MIS-HEMTs and AlGaN/GaN Schottky-gate HEMTs. Benefiting from the PEALD-SiN gate dielectric, the gate leakage current was greatly reduced by about three orders of magnitude up to $V_{gs} = -4$ V for the SiN/AlGaN/GaN MIS-HEMTs, whose reverse gate leakage was as low as 4×10^{-6} mA/mm, lower than 1×10^{-3} mA/mm for the AlGaN/GaN Schottky-gate HEMTs. Moreover, the forward gate leakage current was also well suppressed up to a gate bias of +2 V, resulting in an enlarged gate swing to allow the devices to operate at a larger maximum positive gate voltage to provide a higher maximum output current and saturated power density.

Figure 4(a) shows the output characteristics with V_{gs} swept from −2 to 2 V for the SiN/AlGaN/GaN MIS-HEMTs. The devices exhibit the high maximum drain saturation current densities of 1.2 A/mm. Moreover, the SiN/AlGaN/GaN MIS-HEMTs exhibit a low R_{on} and V_{knee} of 0.6 Ω·mm and 1.2 V, respectively, which attributed to reducing the access and contact resistance of the devices by the small L_{sd} of 0.9 μm and the regrown ohmic contact (0.17 Ω·mm). The excellent on-state characteristics with the high maximum output current density and the low on-resistance, as well as the small knee voltage, proved that the SiN/AlGaN/GaN MIS-HEMTs have the potential to operate at low-voltage RF applications. The breakdown voltage (V_{br}) is defined as the drain voltage corresponding to the drain current density of 1 mA/mm, while the device is biased at the off-state with the gate biased at −8 V and the source biased at 0 V. As demonstrated in Figure 4(b), a V_{br} of 52 V was achieved for the SiN/AlGaN/GaN MIS-HEMTs with L_{sd} of 0.9 μm, which is sufficiently high to meet the low-voltage RF device's need for breakdown voltage. Additionally, it should be noted that the breakdown type of the SiN/AlGaN/GaN MIS-HEMTs is a source-drain breakdown caused by buffer leakage rather than a gate-drain breakdown.

The dynamic performance of the fabricated SiN/AlGaN/GaN MIS-HEMTs is evaluated by the pulsed *I*-*V*. The pulsewidth is 500-ns and the period is 1-ms. Figure 5 shows the pulsed *I*-*V* output of the SiN/AlGaN/GaN MIS-HEMTs with the quiescent bias points of (V_{GSQ}, V_{GSQ}) of (0, 0), (−8, 0), (−8, 10), (−8, 20) and (−8, 30) V. Under the condition of (V_{GSQ}, V_{GSQ}) = (−8, 0) V, the SiN/AlGaN/GaN MIS-HEMTs show a negligible gate delay. A low current collapse of 1.1%, 2.1% and 3.5% was obtained, respectively, at the quiescent bias points of (V_{GSQ}, V_{DSQ}) = (−8, 10), (−8, 20) and (−8, 30) V. The low current collapse of the SiN/AlGaN/GaN MIS-HEMTs is helpful in achieving high PAE and output power in large signal characteristics, which is more suitable for low-voltage RF applications.

To characterize the small signal performance of the SiN/AlGaN/GaN MIS-HEMTs, the S-parameters were measured around the peak Gm and the frequency ranged from 100 MHz to 40 GHz using an Agilent 8363B network analyzer. Figure 6 illustrates the microwave performances of the SiN/AlGaN/GaN MIS-HEMTs, biased at $V_{ds} = 6$ V and V_{gs} for peak transconductance. The maximum current-gain cutoff frequency (f_T) and the maximum power gain cutoff frequency (f_{max}) were obtained by extrapolating the current gain (H_{21}) and the unilateral power gain (UPG) with a −20 dB/decade slope. It can be observed that f_T and f_{max} of the devices were 43 and 120 GHz, respectively. High values of $f_T \times L_g$ (10.75 GHz · μm) and $f_{max} \times L_g$ (30 GHz · μm) were obtained in the fabricated SiN/AlGaN/GaN MIS-HEMTs on Si with $L_g = 0.25$ μm.

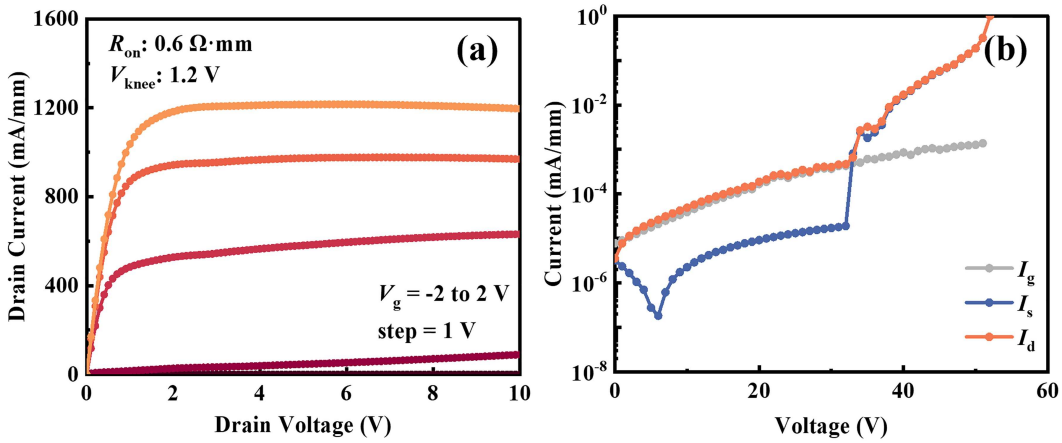

Figure 4 (Color online) (a) Output and (b) three-terminal breakdown characteristics of the SiN/AlGaN/GaN MIS-HEMTs.

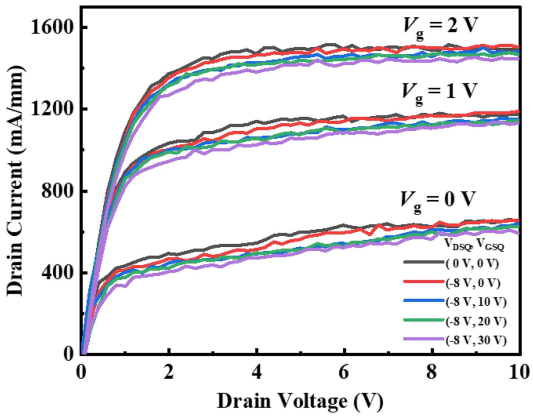

Figure 5 (Color online) Pulse *I*-*V* characteristic at different static biases ((0, 0), (−8, 0), (−8, 10), (−8, 20), and (−8, −30) V) for the SiN/AlGaN/GaN MIS-HEMTs.

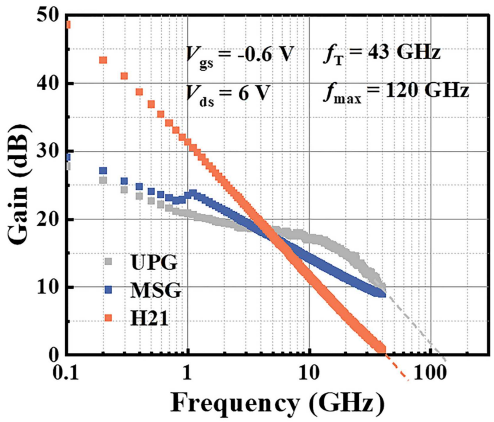

Figure 6 (Color online) Small signal characteristics of the SiN/AlGaN/GaN MIS-HEMTs.

The low-voltage RF power capability characterizations of the SiN/AlGaN/GaN MIS-HEMTs at 3.6 GHz were performed in continuous wave using an on-wafer load-pull system. The load and the source impedance were tuned for optimum PAE. Figure 7 shows the PAE, $P_{\rm out}$, and the power gain as a function of the input power for the SiN/AlGaN/GaN MIS-HEMTs, which were biased at class-AB operation and biased at $V_{\rm ds}$ = 6 and 9 V. It can be observed that the PAE of the SiN/AlGaN/GaN MIS-HEMTs is over 70% at the bias of 6 and 9 V. Specifically, the PAE of 71%, the $P_{\rm out}$ of 0.91 W/mm and the power gain of 16.5 dB were achieved for the SiN/AlGaN/GaN MIS-HEMTs biased at $V_{\rm ds}$ of 6 V. In addition, the PAE as high as 70.6%, the $P_{\rm out}$ of 1.73 W/mm, and the high power gain of 19.1 dB were achieved with bias at $V_{\rm ds}$ = 9 V. The excellent PAE is attributed to the low gate leakage and the high breakdown voltage. The high $P_{\rm out}$ is attributed to the superior dispersion control, the high saturation current, and the low $V_{\rm knee}$ and $R_{\rm on}$. These results suggest that the SiN/AlGaN/GaN MIS-HEMTs demonstrate excellent low-voltage RF power performances.

Figure 8 summarizes the RF power performance of the SiN/AlGaN/GaN MIS-HEMTs compared with the previous reports about GaN-on-Si HEMTs operating at sub-6 GHz band [9–11,34–42], showing that the devices enable both high PAE and output power. To the best of our knowledge, the SiN/AlGaN/GaN MIS-HEMTs fabricated in this work are the first AlGaN/GaN HEMTs on Si substrate with ultrahigh PAE over 70% at the sub-6 GHz band. Meanwhile, the power performance of these devices is better than the AlGaN/GaN HEMTs and comparable to the InAlN/GaN HEMTs and AlN/GaN HEMTs.

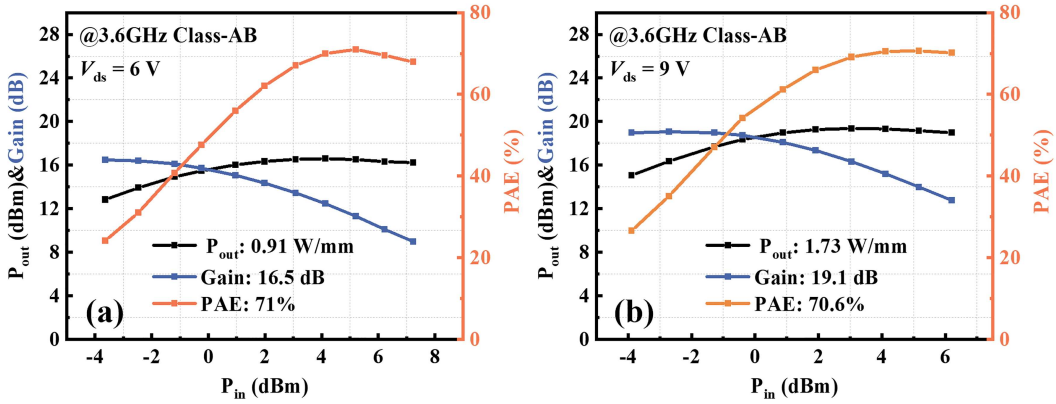

Figure 7 (Color online) Load pull at 3.6 GHz for the SiN/AlGaN/GaN MIS-HEMTs at (a) V_{ds} = 6 V and (b) V_{ds} = 9 V.

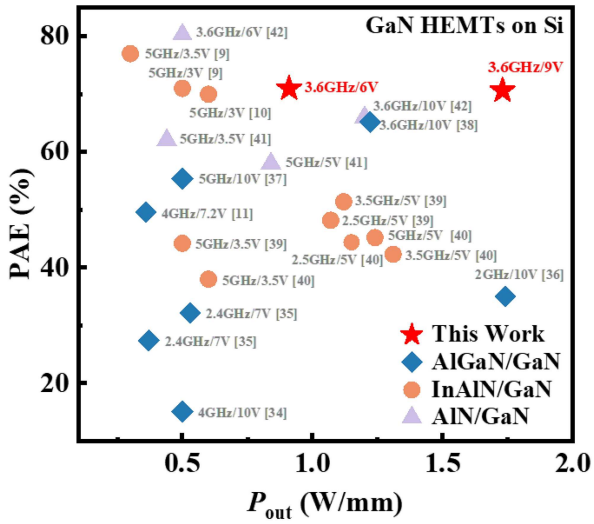

Figure 8 (Color online) Benchmark of low-voltage RF power performance for GaN HEMTs on Si substrate measured $\leqslant$ 10 V and within sub-6-GHz band.

4 Conclusion

High-performance SiN/AlGaN/GaN MIS-HEMTs were achieved using LPCVD-SiN passivation layer, regrown ohmic technology, PEALD-SiN gate dielectric, and scaling down the source-drain distance. The devices exhibit excellent performances with a low R_{on} of 0.6 Ω·mm, a low V_{knee} of 1.2 V, a high on/off current ratio of 5 × 10^7, and a high current density of 1.2 A/mm. The f_T/f_{max} values of 43/120 GHz were obtained in the devices with L_g = 250 nm, delivering a high $f_T \times L_g$ value of 10.75 GHz · μm and a high $f_{max} \times L_g$ value of 30 GHz · μm. At the operating frequency of 3.6 GHz, a PAE of 71% accompanied with a maximum output power density of 0.91 W/mm and an associated gain of 16.5 dB, as well as a peak PAE of 70.6% accompanied with a P_{out} of 1.73 W/mm and an associated gain of 19.1 dB were obtained for the SiN/AlGaN/GaN MIS-HEMTs when biased at V_{ds} = 6 and 9 V, respectively. These results prove that the SiN/AlGaN/GaN MIS-HEMTs have great potential in low-voltage RF applications.

Acknowledgements This work was supported in part by Fundamental Research Funds for the Central Universities (Grant No. YJSJ25013) and National Natural Science Foundation of China (Grant Nos. 62188102, 62174125, 62131014)

References

1 Hao Y, Yang L, Ma X, et al. High-performance microwave gate-recessed AlGaN/AlN/GaN MOS-HEMT with 73% power-added efficiency. IEEE Electron Device Lett, 2011, 32: 626–628
2 Zhang H C, Sun Y, Hu K P, et al. Boosted high-temperature electrical characteristics of AlGaN/GaN HEMTs with rationally designed compositionally graded AlGaN back barriers. Sci China Inf Sci, 2023, 66: 182405
3 Mishra U K, Shen Likun U K, Kazior T E, et al. GaN-based RF power devices and amplifiers. Proc IEEE, 2008, 96: 287–305
4 Wu Y F, Moore M, Saxler A, et al. 40-W/mm double field-plated GaN HEMTs. In: Proceedings of the 64th Device Research Conference, State College, 2006

5 Saito W, Nitta T, Kakiuchi Y, et al. On-resistance modulation of high voltage GaN HEMT on sapphire substrate under high applied voltage. IEEE Electron Device Lett, 2007, 28: 676–678
6 Akira K, Asano T, Tokuda H, et al. High-voltage AlGaN/GaN HEMTs fabricated on free-standing GaN substrates. In: Proceedings of the International Meeting for Future of Electron Devices, Suita, 2013
7 Ohara S, Yamada H, Iwai T, et al. InGaP/GaAs power HBTs with a low bias voltage. In: Proceedings of the International Electron Devices Meeting (IEDM), Washington, 1995
8 Chen S H, Chang L, Chang E Y, et al. High power $Al_{0.3}Ga_{0.7}As/In_{0.2}Ga_{0.8}$ as enhancement-mode PHEMT for low-voltage wireless communication systems. Electron Lett, 2002, 38: 1063–1064
9 Then H W, Radosavljevic M, Jun K, et al. Gallium nitride and silicon transistors on 300 mm silicon wafers enabled by 3-D monolithic heterogeneous integration. IEEE Trans Electron Device, 2020, 67: 5306–5314
10 Then H W, Dasgupta S, Radosavljevic M, et al. 3D heterogeneous integration of high performance high-K metal gate GaN NMOS and Si PMOS transistors on 300mm high-resistivity Si substrate for energy-efficient and compact power delivery, RF (5G and beyond) and SoC applications. In: Proceedings of the International Electron Devices Meeting (IEDM), San Francisco, 2019
11 Zheng Z, Song W, Lei J, et al. GaN HEMT with convergent channel for low intrinsic knee voltage. IEEE Electron Device Lett, 2020, 41: 1304–1307
12 Then H W, Chow L A, Dasgupta S, et al. High-performance low-leakage enhancement-mode high-K dielectric GaN MOSHEMTs for energy-efficient, compact voltage regulators and RF power amplifiers for low-power mobile SoCs. In: Proceedings of the Symposium on VLSI Technology (VLSI Technology), Kyoto, 2015
13 Zhang S, Liu X, Wei K, et al. Suppression of gate leakage current in Ka-band AlGaN/GaN HEMT with 5-nm SiN gate dielectric grown by plasma-enhanced ALD. IEEE Trans Electron Dev, 2021, 68: 49–52
14 Srikanth K, Kushwah B, Dutta G, et al. AlInN/GaN MIS-HEMTs with high pressure oxidized aluminium as gate dielectric. In: Proceedings of the International Conference on Electronics, Computing and Communication Technologies (CONECCT), Bangalore, 2018
15 Liu S, Zhu J, Guo J, et al. Improved breakdown voltage and low damage E-mode operation of AlON/AlN/GaN HEMTs using plasma oxidation treatment. IEEE Electron Device Lett, 2022, 43: 1621–1624
16 Denninghoff D J, Dasgupta S, Lu J, et al. Design of high-aspect-ratio T-gates on N-polar GaN/AlGaN MIS-HEMTs for high $f_{\max}$. IEEE Electron Device Lett, 2012, 33: 785–787
17 Tang Y, Shinohara K, Regan D, et al. Ultrahigh-speed GaN high-electron-mobility transistors with $f_T/f_{\max}$ of 454/444 GHz. IEEE Electron Device Lett, 2015, 36: 549–551
18 Recht F, McCarthy L, Rajan S, et al. Nonalloyed ohmic contacts in AlGaN/GaN HEMTs by ion implantation with reduced activation annealing temperature. IEEE Electron Device Lett, 2006, 27: 205–207
19 Zimmermann T, Deen D, Cao Y, et al. AlN/GaN insulated-gate HEMTs with 2.3 A/mm output current and 480 mS/mm transconductance. IEEE Electron Device Lett, 2008, 29: 661–664
20 Yue Y, Hu Z, Guo J, et al. InAlN/AlN/GaN HEMTs with regrown ohmic contacts and f_T of 370 GHz. IEEE Electron Device Lett, 2012, 33: 988–990
21 Mounika B, Ajayan J, Bhattacharya S, et al. Recent developments in materials, architectures and processing of AlGaN/GaN HEMTs for future RF and power electronic applications: a critical review. Micro Nanostruct, 2022, 168: 207317
22 Ajayan J, Nirmal D, Mohankumar P, et al. Challenges in material processing and reliability issues in AlGaN/GaN HEMTs on silicon wafers for future RF power electronics & switching applications: a critical review. Mater Sci Semiconductor Process, 2022, 151: 106982
23 Binari S C, Klein P B, Kazior T E. Trapping effects in GaN and SiC microwave FETs. Proc IEEE, 2002, 90: 1048–1058
24 Ranjan K, Arulkumaran S, Ng G I, et al. Investigation of self-heating effect on DC and RF performances in AlGaN/GaN HEMTs on CVD-Diamond. IEEE J Electron Device Soc, 2019, 7: 1264–1269
25 Soni A, Ajay A, Shrivastava M. Novel drain-connected field plate GaN HEMT designs for improved $V_{\rm BD}$-$R_{\rm ON}$ tradeoff and RF PA performance. IEEE Trans Electron Device, 2020, 67: 1718–1725
26 Gustafsson S, Jr-Tai Chen S, Bergsten J, et al. Dispersive effects in microwave AlGaN/AlN/GaN HEMTs with carbon-doped buffer. IEEE Trans Electron Device, 2015, 62: 2162–2169
27 Liu Z, Xie H, Lee K H, et al. GaN HEMTs with breakdown voltage of 2200 V realized on a 200 mm GaN-on-insulator (GNOI)-on-Si wafer. In: Proceedings of the Symposium on VLSI Technology (VLSI Technology), 2019
28 Xing W, Liu Z, Qiu H, et al. Planar-nanostrip-channel InAlN/GaN HEMTs on Si with improved g_m and $f_{\rm T}$ linearity. IEEE Electron Device Lett, 2017, 38: 619–622
29 Altuntas P, Lecourt F, Cutivet A, et al. Power performance at 40 GHz of AlGaN/GaN high-electron mobility transistors grown by molecular beam epitaxy on Si(111) substrate. IEEE Electron Device Lett, 2015, 36: 303–305
30 de Jaeger B, van Hove M, Wellekens D, et al. Au-free CMOS-compatible AlGaN/GaN HEMT processing on 200 mm Si substrates. In: Proceedings of the International Symposium on Power Semiconductor Devices and ICs, Bruges, 2012
31 Parvais B, Alian A, Peralagu U, et al. GaN-on-Si Mm-wave RF devices integrated in a 200mm CMOS compatible 3-level Cu BEOL. In: Proceedings of the International Electron Devices Meeting (IEDM), San Francisco, 2020
32 Kotani J, Yaita J, Homma K, et al. 24.4 W/mm X-band GaN HEMTs on AlN substrates with the LPCVD-Grown high-breakdown-field SiN_xlayer. IEEE J Electron Device Soc, 2023, 11: 101–106
33 Shi Y, Huang S, Bao Q, et al. Normally OFF GaN-on-Si MIS-HEMTs fabricated with LPCVD-SiN_x passivation and high-temperature gate recess. IEEE Trans Electron Device, 2016, 63: 614–619
34 Chumbes E M, Shealy J R, Schremer A T, et al. AlGaN/GaN high electron mobility transistors on Si(111) substrates. IEEE Trans Electron Device, 2001, 48: 420–426
35 Liu H Y, Lee C S, Hsu W C, et al. Investigations of AlGaN/AlN/GaN MOS-HEMTs on Si substrate by ozone water oxidation method. IEEE Trans Electron Device, 2013, 60: 2231–2237
36 Bose A, Biswas D, Hishiki S, et al. A temperature stable amplifier characteristics of AlGaN/GaN HEMTs on 3C-SiC/Si. IEEE Access, 2021, 9: 57046–57053
37 Cheng Y, Ng Y H, Zheng Z, et al. RF enhancement-mode p-GaN gate HEMT on 200 mm-Si substrates. IEEE Electron Device Lett, 2023, 44: 29–31
38 Lu H, Hou B, Yang L, et al. High RF performance GaN-on-Si HEMTs with passivation implanted termination. IEEE Electron Device Lett, 2022, 43: 188–191
39 Xie H, Liu Z, Hu W, et al. GaN-on-Si HEMTs fabricated with Si CMOS-compatible metallization for power amplifiers in low-power mobile SoCs. IEEE Microw Wireless Compon Lett, 2021, 31: 141–144
40 Xie H, Liu Z, Hu W, et al. CMOS-compatible InAlN/GaN HEMTs on silicon for RF power amplifiers in 5G mobile SoCs. In: Proceedings of the MTT-S International Microwave Workshop Series on Advanced Materials and Processes for RF and THz Applications (IMWS-AMP), 2021: 397–399
41 Xie H, Liu Z, Hu W, et al. AlN/GaN MISHEMTs on Si with in-situ SiN as a gate dielectric for power amplifiers in mobile SoCs. Appl Phys Express, 2022, 15: 016503
42 Gao G, Liu Z, Hao L, et al. E-mode AlN/GaN HEMTs on Si with 80.4% PAE at 3.6 GHz for low-supply-voltage RF power applications. IEEE Electron Device Lett, 2025, 46: 40–43